Title

Mouse and human immune responses share neutralization epitopes of HAstV-VA1

Journal

Journal of Virology, 98(7)

ISSN

0022-538X

Authors

Ramírez-Bello, Inci

López, Tomás

Espinosa, Rafaela

et al.

Publication Date

2024-07-23

DOI

10.1128/jvi.00971-24

Peer reviewed

Journal of Virology

Virology | Full-Length Text

Mouse and human immune responses share neutralization epitopes of HAstV-VA1

Inci Ramírez-Bello,[1] Tomás López,[1] Rafaela Espinosa,[1] Anisa Ghosh,[2,3] Kassidy Green,[2,3] Lidia Riaño-Umbarila,[1,2] Carlos Gaspar-Castillo,[4] Catalina Aguilera-Flores,[1] Celia M. Alpuche-Aranda,[4] Susana López,[1] Rebecca M. DuBois,[2,3] Carlos F. Arias[1]

AUTHOR AFFILIATIONS See affiliation list on p. 15.

ABSTRACT Astroviruses are highly divergent and infect a wide variety of animal hosts. In 2009, a genetically divergent human astrovirus (HAstV) strain VA1 was first identified in an outbreak of acute gastroenteritis. This strain has also been associated with fatal central nervous system disease. In this work, we report the isolation of three high-affinity neutralizing monoclonal antibodies (Nt-MAbs) targeting the capsid spike domain of HAstV-VA1. These antibodies (7C8, 2A2, 3D8) were used to select individual HAstV-VA1 mutants resistant to their neutralizing activity and a HAstV-VA1 triple mutant that escapes neutralization from all three Nt-MAbs. Sequencing of the virus genome capsid region revealed escape mutations that map to the surface of the capsid spike domain, define three potentially independent neutralization epitopes, and help delineate four antigenic sites in human astroviruses. Notably, two of the escape mutations were found to be present in the spike sequence of the HAstV-VA1-PS strain isolated from an immunodeficient patient with encephalitis, suggesting that those mutations arose as a result of the immune pressure generated by the patient's immunotherapy. In agreement with this observation, human serum samples exhibiting strong neutralization activity against wild-type HAstV-VA1 had a 2.6-fold reduction in neutralization titer when evaluated against the triple-escape HAstV-VA1 mutant, suggesting that both mouse and human antibody responses target shared neutralization epitopes. The isolated Nt-MAbs reported in this work will help to characterize the functional domains of the virus during cell entry and have the potential for developing a specific antibody therapy for the neurological disease associated with HAstV-VA1.

IMPORTANCE Human astroviruses (HAstVs) have been historically associated with acute gastroenteritis. However, the genetically divergent HAstV-VA1 strain has been associated with central nervous system disease. In this work high-affinity neutralizing monoclonal antibodies directed to HAstV-VA1 were isolated and characterized. The proposed binding sites for these antibodies and for neutralizing antibodies against classical HAstVs suggest that there are at least four neutralization sites on the capsid spike of astroviruses. Our data show that natural infection with human astrovirus VA1 elicits a robust humoral immune response that targets the same antigenic sites recognized by the mouse monoclonal antibodies and strongly suggests the emergence of a variant HAstV-VA1 virus in an immunodeficient patient with prolonged astrovirus infection. The isolated Nt-MAb reported in this work will help to define the functional sites of the virus involved in cell entry and hold promise for developing a specific antibody therapy for the neurological disease associated with HAstV-VA1.

KEYWORDS VA1 astrovirus, neutralizing monoclonal antibody, epitope mapping, immunodeficient patient

Editor Christiane E. Wobus, University of Michigan Medical School, Ann Arbor, Michigan, USA

Address correspondence to Carlos F. Arias, arias@ibt.unam.mx.

The authors declare no conflict of interest.

See the funding table on p. 16.

Received 4 June 2024
Accepted 5 June 2024
Published 25 June 2024

Human astroviruses (HAstVs), first identified in 1975, are significant etiological agents of infantile gastroenteritis and are also associated with diarrheal disease in the elderly and immunocompromised people (1–3). The initially recognized HAstV strains were classified into eight serotypes currently known as classical HAstVs within the *Mamastrovirus 1* species in the *Mammastrovirus* genus of the Astroviridae family. Beginning in 2008, astrovirus strains, genetically closer to bovine, ovine, and porcine astroviruses rather than to classical HAstVs, were reported in human feces (4–6). These nonclassical HAstVs (MLB and VA) group into two different clades and are classified into three astrovirus species: *Mamastrovirus 6* (MLB1, MLB2, and MLB3), *Mamastrovirus 8* (VA2, VA4, VA5, and BF34), and *Mamastrovirus 9* (VA1 and VA3) (2). The association of viruses in the MLB and VA clades with gastroenteritis has not been conclusively demonstrated (2). However, they commonly infect humans, with a reported seropositivity rate of up to 100% in adult populations (7, 8).

More recently, HAstVs have been associated with meningitis and encephalitis in immunocompromised patients, with HAstV-VA1 (hereafter referred also as VA1) being the most frequently detected virus in these cases [see references in reference (9)]. Also, a growing number of newly identified neurotropic astroviruses have been identified in cases of nonsuppurative encephalitis and neurological disease in pigs, ruminant species (cattle, sheep), and minks, changing the perception of the role of these viruses in non-enteric diseases (10). Mammalian astroviruses have high genetic diversity, are highly ubiquitous, and have a broad host range (11). Evolutionary analyses suggest that sustained and extensive cross-species transmission events have occurred in the past between wild and domestic animal species and humans (11–14). In this context, studying human and animal astroviruses is warranted as part of a One Health approach and in preparation for future zoonotic events.

HAstVs are small, nonenveloped viruses with a single-stranded, positive-sense RNA genome of approximately 6.7 kb (2, 3). In the case of the nonclassical VA1 strain, the capsid of the mature, infectious virion is composed of two polypeptides: VP33, which constitutes the shell of the virus particle (basic region and inner core structural domain), and VP38, which includes the dimeric globular spikes that protrude from the virion (outer core and spike structural domains) (15). These two polypeptides are derived from a capsid precursor protein of 86 kDa (VP86) processed intracellularly by an undefined protease (15). Previously, the antigenic sites of neutralizing monoclonal antibodies (Nt-MAbs) to the capsid spike domain of classical HAstVs have been mapped (16–18). However, despite the medical relevance of the non-classical HAstV-VA1, there is limited information about its antigenic sites. Its characterization should help identify immunoreactive regions or epitopes as the basis of protective immunity and teach about functional sites on the virus capsid.

In this work, we report the isolation of three Nt-MAbs targeting HAstV-VA1. We identified mutations in the spike domain enabling the virus to escape neutralization by these MAbs, delineating three potentially independent neutralization sites. We also show that mouse and human neutralizing humoral immune responses target these antigenic regions. This study broadens our knowledge about the neutralization antigenic structure of HAstVs, including those more closely related to animal viruses, such as VA1. It contributes to a more panoramic view of the functional sites of the virus capsid involved in the initial interactions of the virus with its host cell and provides the basis for developing targeted antibody therapy for neurological diseases associated with HAstV-VA1.

RESULTS

HAstV-VA1 neutralization epitopes reside on the capsid spike domain

Previously, we reported that neutralization epitopes for classical human astrovirus serotypes 1, 2, and 8 are located on the capsid spike domain (17). To investigate if this is also the case for astrovirus HAstV-VA1, which belongs to a different clade than classical HAstVs, we evaluated the capacity of different regions of the HAstV-VA1 capsid to

elicit virus-neutralizing antibodies (Nt-Abs). Rabbits were immunized with recombinant polypeptides corresponding to a fragment of the core structural domain (α-core, amino acids 180–300), the spike structural domain (α-spike, amino acids 408–684) proteins, and the core structural domain (α-DB, amino acids 71–406) (Fig. 1A). Antibodies directed to the virus capsid spike (anti-Spike) efficiently neutralized the infectivity of HAstV-VA1 (Fig. 1B). In contrast, antibodies raised to the other two recombinant core-related proteins did not have neutralizing activity (Fig. 1B). These results strongly suggest that for HAstV-VA1, most neutralization epitopes reside on the capsid spike domain, as it is in classical HAstVs.

Isolation and characterization of neutralizing monoclonal antibodies to HAstV-VA1

To isolate Nt-MAbs against HAstV-VA1, BALB/C mice were immunized with HAstV-VA1 particles purified by CsCl isopycnic density centrifugation. Screening for hybridomas-secreting antibodies to the virus was carried out by ELISA using purified virus particles as antigen, and positive hybridomas were subsequently tested in a neutralization assay. Three stable hybridomas-secreting Nt-MAbs, 7C8, 2A2, and 3D8 were identified. Ascitic fluids were produced in mice, and their antibody isotype was determined: 7C8 (IgG_1),

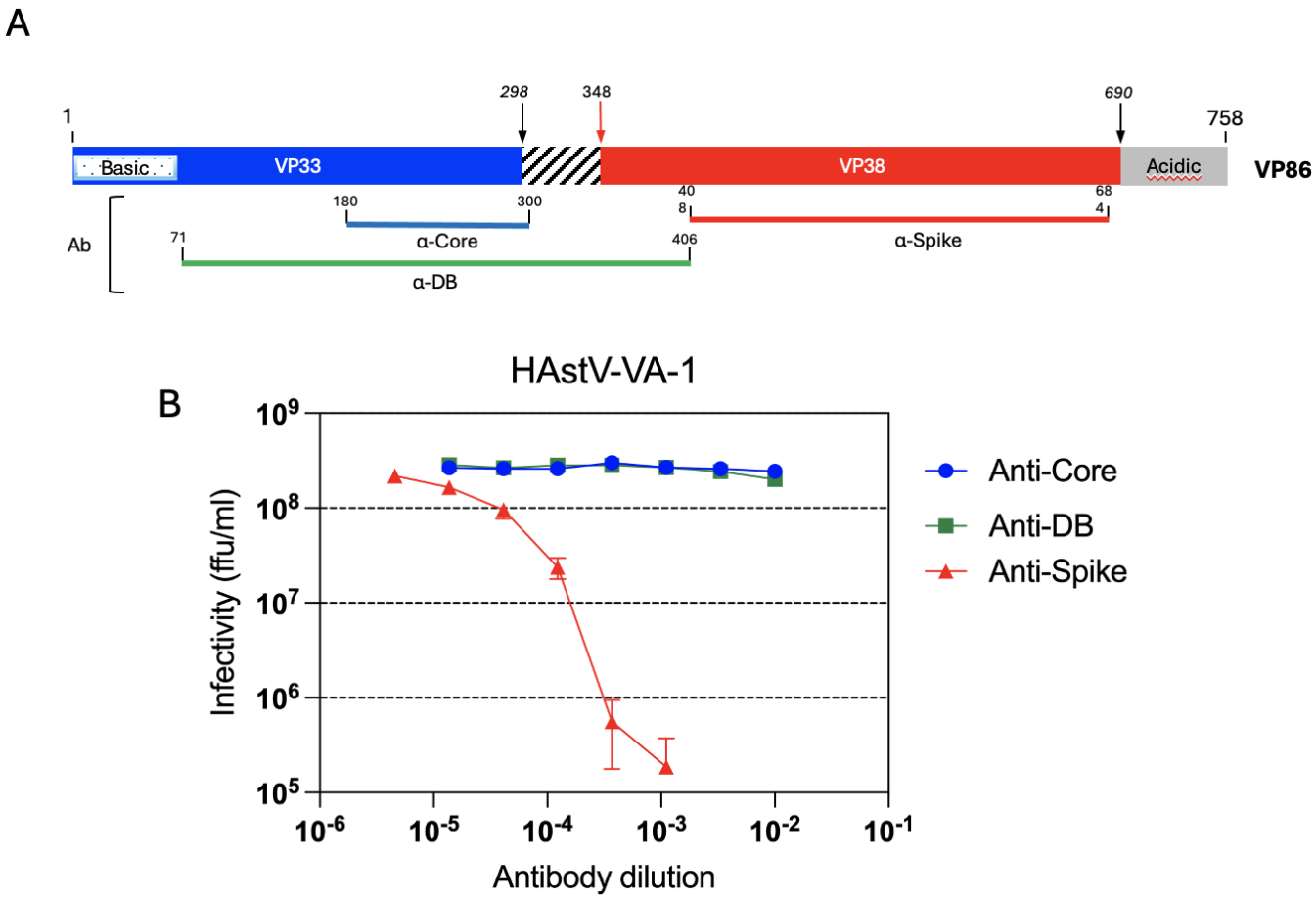

FIG 1 (A) Diagram of the VA1 ORF2 capsid precursor and recombinant proteins. ORF2 is represented as a box. The position of the VP33 and VP38 proteins is indicated. The hatched box indicates a region in which its termini are proteolytically cleaved. The recombinant proteins used to generate antibodies are represented as blue (Core), red (Spike), and green (DB) lines. The diagram is to scale. The numbers indicate the VA1 ORF2 amino acids included in each recombinant protein. α-Core, α-spike, and α-DB stand for the sera raised against the corresponding protein. (B) Induction of neutralizing antibodies by recombinant core, spike, and DB proteins. HAstV-VA1 was preincubated with rabbit anti-core or anti-DB hyperimmune sera or with mouse anti-spike hyperimmune serum at the indicated dilutions, and the infectivity of the virus was determined as described in Materials and Methods. The infectivity assay was performed in biological triplicates and carried out in duplicate. The data are expressed as focus-forming units (ffu)/mL and represent the mean ± SEM.

2A2 (IgG_{2a}), and 3D8 (IgG_{2a}). All antibodies seem to recognize conformational epitopes since they did not interact with the VA1 spike by Western blot.

On the other hand, all three MAbs efficiently neutralized virus infectivity at dilutions similar to those obtained with a mouse polyclonal antibody to the virus (Fig. 2A). In addition, they could efficiently detect infected cells by immunofluorescence (Fig. 2B) at 24 h post-infection (hpi), with most of the signal presumably corresponding to particles partially inside or at the edges of the vesicles induced during virus infection, as has been previously reported (19, 20). Ascitic fluids of Nt-MAb to classical HAstV serotypes 1, 2, and 8 (17), which do not neutralize the infectivity of VA1 (Fig. 2A), served as negative controls. On the other hand, MAbs 7C8, 2A2, and 3D8 did not neutralize either classical HAstVs serotypes 1 and 8, or HAstV-MLB1 (Fig. 2C). These observations were not unexpected since HAstV VA1, MLB1, and classical viruses belong to three different astrovirus species (2).

Neutralizing antibodies to HAstV-VA1 have a high affinity for the capsid spike

The affinity of MAbs 7C8, 2A2, and 3D8 for recombinant HAstV-VA1 capsid spike was determined by biolayer interferometry (BLI). Anti-Mouse IgG Fc Capture (AMC) biosensors coated with either MAb 7C8, 2A2, or 3D8 were dipped into wells containing 1:2 serially diluted recombinant HAstV-VA1 spike domain in assay buffer to determine the association rate. Biosensors were then dipped in assay buffer to determine the dissociation rate. We found that all three MAbs bind with high affinity to the HAstV-VA1 spike, with dissociation constants (KD) of 1.2 nM for MAb 2A2, 0.4 nM for MAb 7C8, and 1.9 nM for MAb 3D8 (Fig. 3A through C). The KD values correlate with the neutralization activity

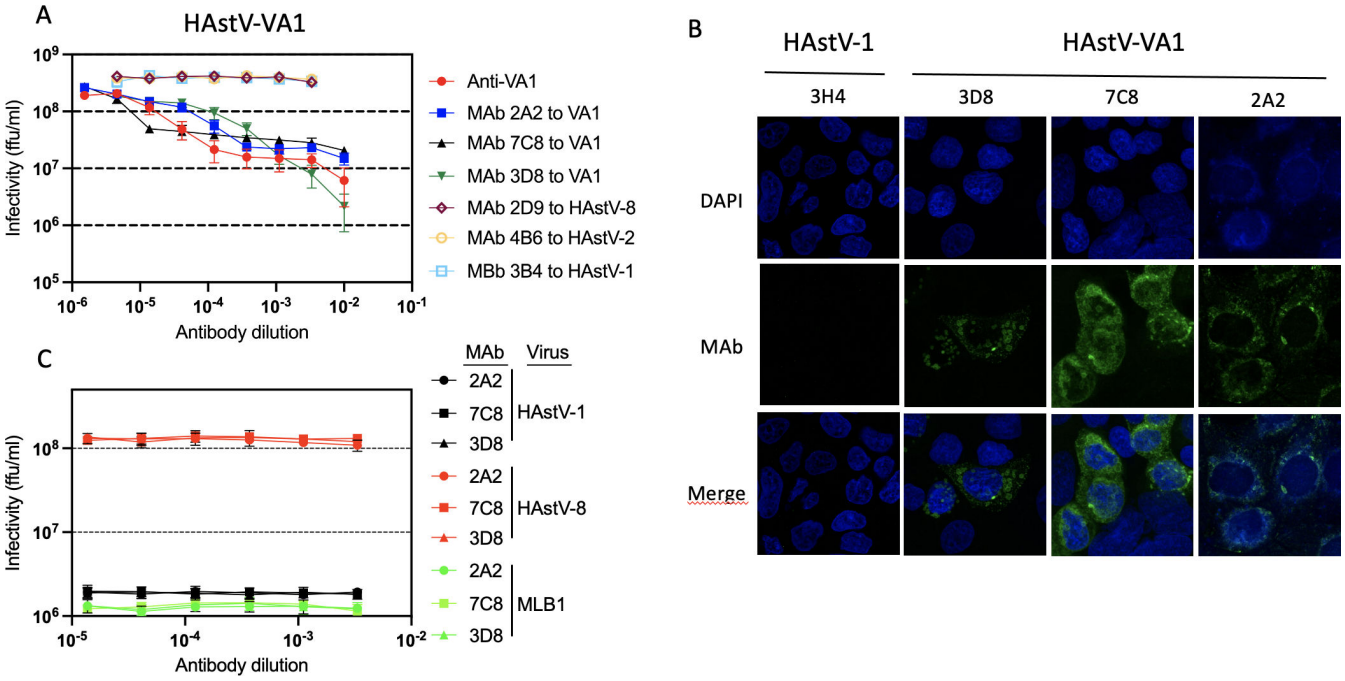

FIG 2 Neutralization activity of monoclonal antibodies. (A) HAstV-VA1 was preincubated with mouse ascitic fluid of MAbs 2A2, 7C8, or 3D8 or with mouse hyperimmune polyclonal serum to VA1 virus particles (Anti-VA1) at the indicated dilutions. As a negative control, we used mouse ascitic fluid for either Nt-MAb 3B4 to HAstV-1, 4B6 to HAstV-2, or 2D9 to HAstV-8. The infectivity of the virus was determined as described in Materials and Methods. The infectivity assay was performed in biological triplicates and carried out in duplicate. The data are expressed as focus-forming units (ffu)/mL and represent the mean ± SEM. (B) Caco-2 cells were infected with HAstV-VA1 at a multiplicity of infection of 0.5, and at 24 hpi, they were fixed with formaldehyde and incubated with MAbs 2A2, 7C8, or 3D8. MAb 3H4 to HAstV-1 was used as the negative control since it does not cross-react with VA1. The cells were subsequently incubated with Alexa 488-labeled anti-IgG antibodies and observed for immunofluorescence as described in Materials and Methods. Nuclei were stained with DAPI. (C) The ascitic fluid of Nt-MAbs 2A2, 7C8, and 3D8 was preincubated with classical HAstV serotype 1 or 8 and with the divergent HAstVs MLB1, and their infectivity was determined as described in Materials and Methods.

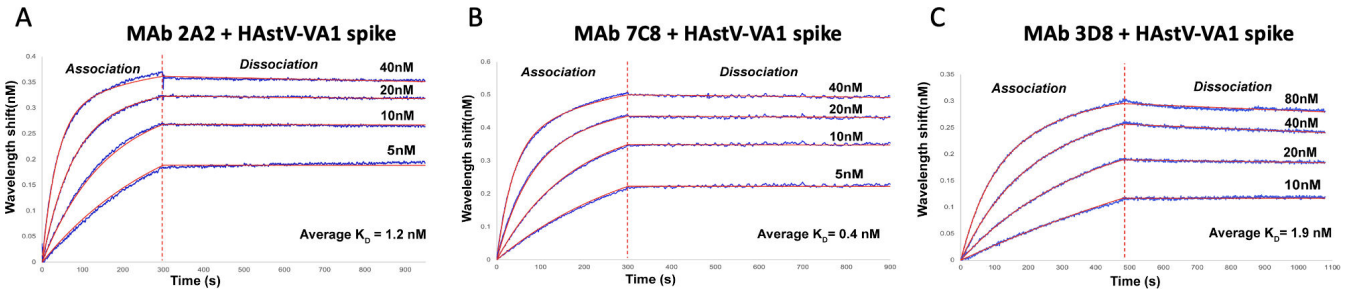

FIG 3 Binding affinities of mAbs 2A2, 7C8, and 3D8 to HAstV-VA1 capsid spike. (A) mAb 2A2, (B) 7C8, or (C) 3D8 was loaded onto biosensors and then placed into 1:2 serial dilutions of HAstV-VA1 spike at the indicated concentrations to allow association and then placed into assay buffer to allow dissociation. Representative traces of the data are shown. The KD value represents the mean of two independent experiments.

of the MAbs. Thus, MAb 7C8 shows the highest neutralization activity (Fig. 2A) and the lowest KD (Fig. 3B). Similarly, MAb 3D8 shows the lowest neutralization activity (Fig. 2A) and the highest KD (Fig. 3C), suggesting that the Nt-MAb affinity of the MAbs is a relevant factor for their neutralization activity.

Selection of HAstV-VA1 mutants that escape MAb neutralization

To determine the potential binding sites for the isolated Nt-MAbs, virus mutants that escaped neutralization were isolated after at least three virus passages grown in the presence of the corresponding Nt-MAb. As shown in Fig. 4, mutants that efficiently escaped neutralization by the cognate MAb were successfully selected. However, escape mutant m3D8 was still somewhat sensitive to neutralization at high MAb 3D8 concentrations (Fig. 4C). All three escape mutants were neutralized by the other two MAbs, suggesting that the three antibodies recognize different epitopes on the virus spike. In addition, all three escape mutants were neutralized similarly by the polyclonal antibody to HAstV-VA1 (Fig. 4D).

A double-escape mutant resistant to neutralization by both 7C8 and 2A2 MAbs was isolated (Fig. 5A). This double mutant (m7C8/m2A2) was sensitive to neutralization by MAb 3D8 and by the polyclonal antibody to HAstV-VA1 (Fig. 5A), confirming the independence of at least three neutralization antigenic sites on the virus spike. A virus mutant that escaped neutralization by all three Nt-Mabs was also isolated, using the 7C8/2A2 double mutant as the starting virus and selecting a virus resistant to neutralization by MAb 3D8 (Fig. 5B). Interestingly, this triple mutant was fully resistant to 3D8 neutralization and maintained its resistance to MAb 7C8; however, it became slightly sensitive to neutralization by MAb 2A2 (Fig. 5B), indicating that the mutation selected by MAb 3D8 somehow facilitated the interaction of this triple mutant with MAb 2A2. It is important to point out, however, that 50% inhibition of the triple mutant by MAb 2A2 was reached at about a 1:300 dilution of the 2A2 ascites fluid (Fig. 5B). In comparison, 50% inhibition of the wild-type virus with the 2A2 ascitic fluid was obtained with about a 1:50,000 dilution (Fig. 2A), showing that the triple mutant was still very refractory to neutralization by all three Nt-MAbs. Finally, VA1 polyclonal serum was still effective in neutralization of the triple-escape mutant, suggesting that there is at least a fourth neutralization epitope on the HAstV-VA1 spike, different from the epitopes recognized by the three Nt-MAbs characterized in this work.

Of interest, growth curves carried out for the single-, double-, and triple-escape mutants (Fig. 5C) show that all mutants have similar replication cycles and also reach similar infectious titers at 48 hpi. These observations suggest that the VA1 spike protein has the plasticity to maintain its function even when mutations at sites of interaction with Nt-MAbs occur.

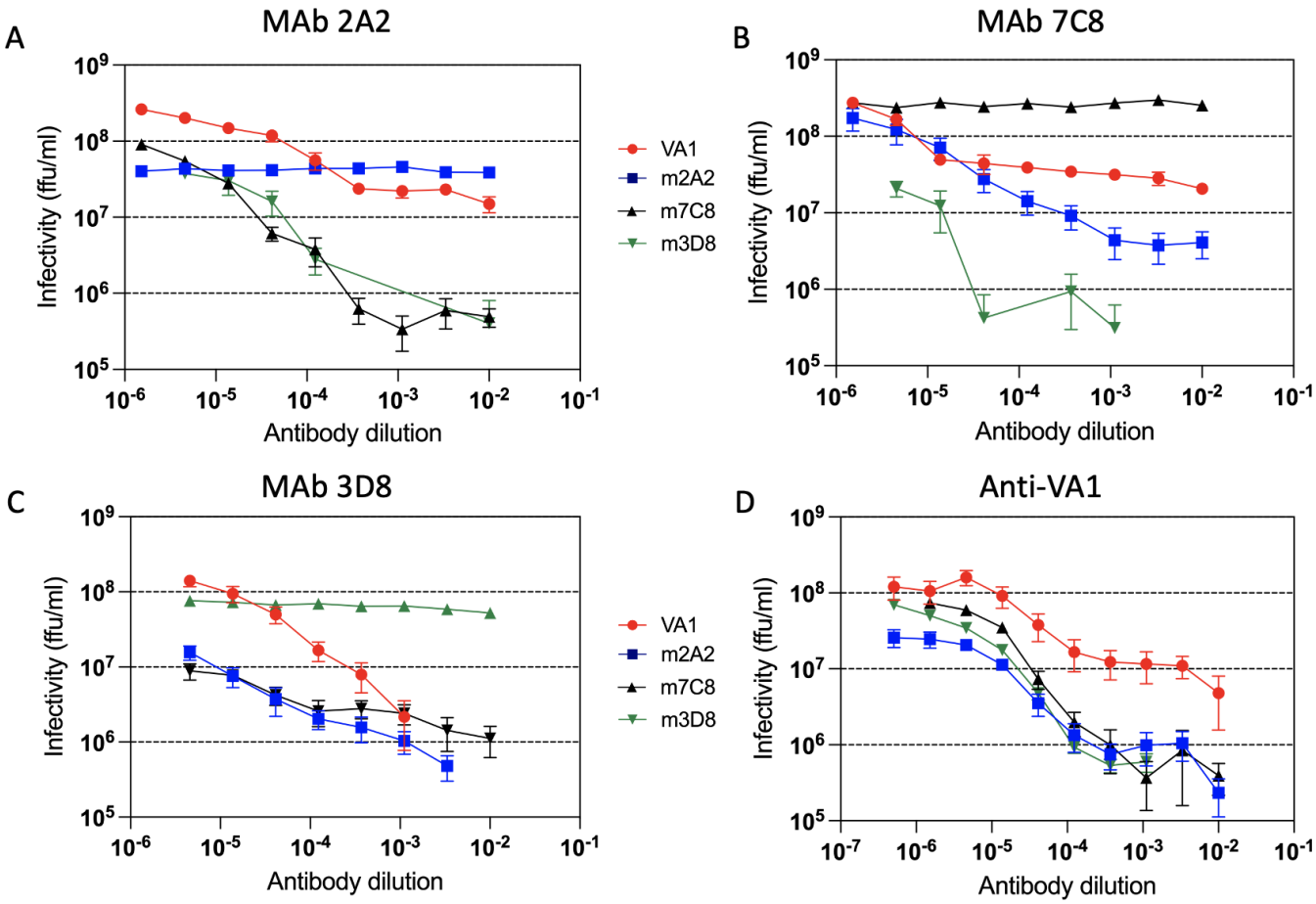

FIG 4 Neutralization of HAstV-VA1 escape variants. Escape variants m2A2, m7C8, m3D8, or wild-type HAstV-VA1 were preincubated with MAbs 2A2 (A), 7C8 (B), or 3D8 (C), or with mouse anti-VA1 polyclonal serum (D) at the indicated dilutions, and the infectivity of the virus was determined as described in Materials and Methods. The infectivity assay was performed in biological triplicates and carried out in duplicate. Data are expressed as focus-forming units (ffu)/mL and represent the mean ± SEM.

Identifying the mutations that allow HAstV-VA1 to escape mAb neutralization

To determine the amino acid changes that conferred HAstV-VA1 resistance to neutralization by the isolated MAbs, the sequence of the ORF2 region encoding the capsid spike of the wild-type and mutant viruses was determined. The spike sequence corresponding to the wild-type virus in our lab (HAstV-VA1, P14; GenBank #PP236967) has two conservative changes (Y420F and S670T) with respect to the sequence previously reported (GenBank #KY933670). When the P14 VA1 spike wild-type sequence was compared with those obtained from the escape mutants, a single amino acid change was detected on the VA1 mutants m7C8 (P543L) and m3D8 (E564V) spike (Fig. 6A). In contrast, the escape mutant m2A2 showed two amino acid changes separated by four amino acids (S611L and R615G) (Fig. 6A). Of interest, the potential epitopes defined by these escape mutations are highly conserved among the reported VA spike sequences [see Fig. 5 in reference (9)].

The 7C8/2A2 double-escape mutant (m7C8/2A2) showed the S611L and R615G mutations identified in m2A2. However, instead of the P543L mutation detected in m7C8, an Arg to Gly mutation was selected at the neighboring amino acid 542 (R542G). Finally, the triple-escape mutant (m7C8/2A2/3D8) shared R615G and Q541R with the double mutant but acquired a new mutation at amino acid 603 (G603E) and lost the

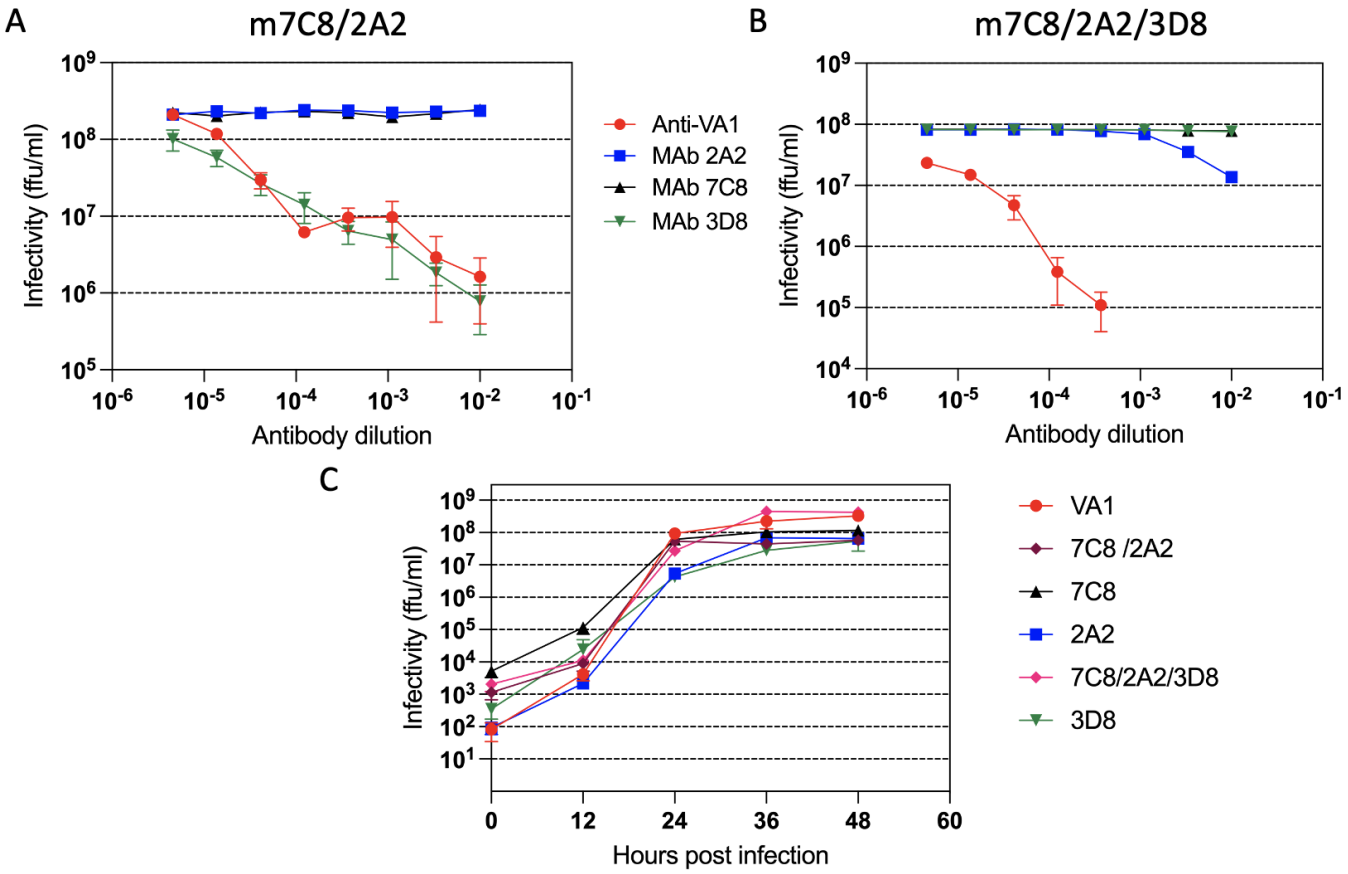

FIG 5 Neutralization of double and triple neutralization escape HAstV-VA1 variants. Double m7C8/2A2 (A) and triple m7C8/2A2/3D8 (B) neutralization-escape variants were preincubated with MAbs 2A2, 7C8, or 3D8 or with mouse anti-VA1 polyclonal serum at the indicated dilutions, and the infectivity of the virus was determined as described in Materials and Methods. The infectivity assay was performed in biological triplicates and carried out in duplicate. Data are expressed as focus-forming units (ffu)/mL and represent the mean ± SEM. (C) Single-cycle replication curve of single-, double-, and triple-escape mutants and wild-type astrovirus VA1. Monolayers of Caco-2 cells were infected with VA1 at a multiplicity of infection of 5 in DMEM-HG, and the infection was left to proceed for the indicated times post-infection at 37°C. At the end of the incubation period, the cell media and the cells were lysed by three cycles of freeze thawing. The virus titer was determined by an immunoperoxidase focus-forming assay as described in Materials and Methods. The infectivity assay was performed in biological duplicates and carried out in quadruplicate. Data are expressed as focus-forming units (ffu)/mL and represent the mean ± SEM.

mutation S611L. These results show the consistency of identification of sites that appear relevant for interaction with Nt-MAbs.

Mapping of escape mutations on the 3D structure of the HAstV-VA1 spike

The 3D structure of the HAstV-VA1 spike has been recently reported (9). All escape mutations were found to be located on the spike surface (Fig. 6A), mapping to the β9-β10 loop (7C8), β10-β11 loop (3D8), and β16-β17 loop (2A2) (Fig. 6B). Escape mutations in viruses m2A2 and m3D8 are located close in space, on one of the faces of the spike. Thus, even though these two mutations appear to be part of two different neutralization epitopes, they could overlap and belong to the same antigenic site. On the other hand, the escape mutation in m7C8 maps in the middle region of the same face of the dimeric spike where 3D8 and 2A2 mutations lie but in the opposite protomer (Fig. 6A). Of interest, the amino acid mutation selected by MAb 3D8 (G603E) in the triple-escape mutant mapped close to the top of the spike but not far from the initial escape mutation in m3D8 (E564V) (Fig. 6A). These results suggest that both lateral sides of each protomer, and possibly the top of the dimeric VA1 spike, are targets of Nt-MAb.

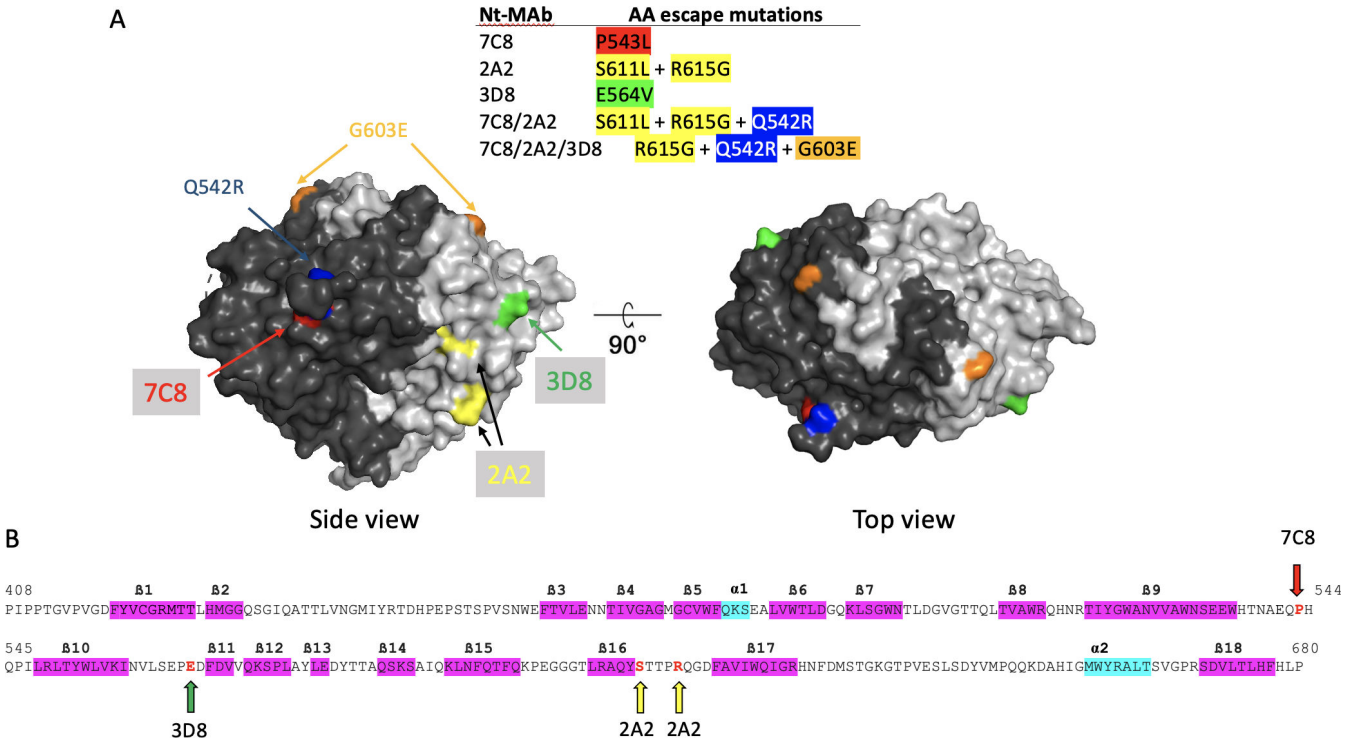

FIG 6 Localization of point mutations that confer escape from neutralization by monoclonal antibodies. (A) The crystal structure of the HAstV-VA1 spike is shown from the top and the side. One half of the dimer is colored dark gray, and the other half is light gray. The mutations that allow wild-type HAstV-VA1 to escape neutralization from the various MAbs are colored green for 3D8, yellow for 2A2, and red for 7C8. The additional mutations identified in the double m7C8/2A2 and triple m7C8/2A2/3D8 escape mutants are colored in blue and gold, respectively. The mutations are shown in only one protomer in the dimer. (B) Sequence of the HAstV-VA1 capsid spike protein (P14 strain). The amino acids that changed in the escape variants are shown in red letters and indicated by red (7C8), green (3D8), or yellow (2A2) arrows. Beta strands are highlighted in magenta and alpha-helices in cyan.

Escape mutations in HAstV-VA1 can also be selected during virus evolution in a prolonged human VA1 infection

It was recently reported that the VA1 spike sequences available in databases can be classified into two distinct groups (9). One group includes the spike sequences of viruses isolated from patients with gastrointestinal disease (VA1-gastro), while the second group contains sequences of viruses isolated from immunocompromised people with neurological disease (VA1-neuro). The recombinant spike domains for strain PS, a VA1-neuro strain (GenBank #ADH93577.1; ref 21), and strain P14, a VA1-gastro strain (GenBank #PP236967) were expressed in *E. coli* and used for binding to the antibodies. Surprisingly, by BLI, MAb 7C8 efficiently bound the P14 spike but not the PS spike (Fig. 7A). Analysis of the spike sequence of the PS VA1-neuro strain showed 21 amino acid changes when compared to the P14 VA1-gastro strain (Fig. 7B). Most interestingly, two contiguous changes in the PS VA1-neuro spike sequence are precisely the escape mutations identified in m7C8 and m7C8/2A2 escape viruses (Q542R and P543L) (Fig. 7B), probably explaining the lack of interaction of MAb7C8 with the PS spike. These findings suggest that these amino acid changes arose in the PS VA1-neuro virus as a response to the neutralizing immune pressure imposed by the immunotherapy with human convalescent sera that the patient received during treatment (21).

The neutralization sites identified in HAstV-VA1 are also targets of Nt-Abs induced during a natural HAstV-VA1 human infection

Considering the previous observation, we evaluated if the neutralization sites identified in HAstV-VA1 with the Nt-MAbs described in this work are also targets for neutralizing antibodies induced during natural infection of HAstV-VA1 in humans. For this, the

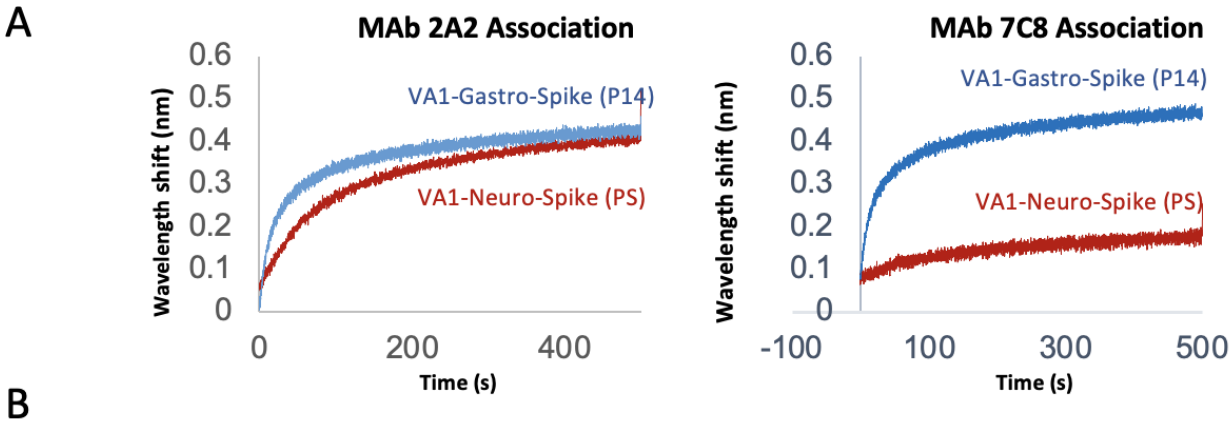

B

```
          350        360        370        380        390        400        410        420
PS        TDDQYLVYASLADAQNNRPVEARDYTRVTCQTTLSSTQINAPNTGPNTTIESIGNNNQQWPIPLTGVPVGDFYVYGRMTT
P14       TDVQYLVYASLADAQNNRPVEAQNYTKVTRQTTLSSTQINAPNTGPNTTTGSIGNNNQQWPIPPTGVPVGDFFVCGRMTT
mP14      TDVQYLVYASLADAQNNRPVEAQNYTKVTRQTTLSSTQINAPNTGPNTTTGSIGNNNQQWPIPPTGVPVGDFFVCGRMTT

          430        440        450        460        470        480        490.       500
PS        LHMGGQSGIQATTLVNGMIYRTDHPEPSTSPVSNWEFTVLENNTIVGAGMGCVWFQKSEVLVWTLDGQKLSGWNTLDGVG
P14       LHMGGQSGIQATTLVNGMIYRTDHPEPSTSPVSNWEFTVLENNTIVGAGMGCVWFQKSEALVWTLDGQKLSGWNTLDGVG
mP14      LHMGGQSGIQATTLVNGMIYRTDHPEPSTSPVSNWEFTVLENNTIVGAGMGCVWFQKSEALVWTLDGQKLSGWNTLDGVG

          510        520        530        540        550        560        570.       580
PS        TTQLTVAWRQHNRTIYGWANVVAWNSEEWHTNAERLHQPTLRLTYWLVKINVSSEPEDFDVVQKFPLAYLEDYTTAQSKS
P14       TTQLTVAWRQHNRTIYGWANVVAWNSEEWHTNAEQPHQPILRLTYWLVKINVLSEPEDFDVVQKSPLAYLEDYTTAQSKS
mP14      TTQLTVAWRQHNRTIYGWANVVAWNSEEWHTNAERLHQPILRLTYWLVKINVLSEPVDFDVVQKSPLAYLEDYTTAQSKS

          590        600        610        620        630        640        650        660
PS        AIQKLNFQTFQKPEGGGTLRAQYSTVPRQGDFAVIWQIGRHNFDMSTGKGTPVESLSDYVMPQQKDARIGMWYRALTSVG
P14       AIQKLNFQTFQKPEGGGTLRAQYSTTPRQGDFAVIWQIGRHNFDMSTGKGTPVESLSDYVMPQQKDAHIGMWYRALTSVG
mP14      AIQKLNFQTFQKPEGEGTLRAQYLTTPGQGDFAVIWQIGRHNFDMSTGKGTPVESLSDYVMPQQKDAHIGMWYRALTSVG

          670.       680
PS        PRSDMLTLHFHFP
P14       PRTDVLTLHFHLP
mP14      PRTDVLTLHFHLP
```

FIG 7 (A) Binding affinities of mAbs 7C8 and 2A2 to VA1 capsid spikes PS (VA1-neuro spike) and P14 (VA1-gastro spike). MAbs were loaded onto biosensors and then placed into a 20 nM solution of the corresponding HAstV-VA1 spike to allow association. Representative traces of experiments performed in triplicate are shown. (B) Comparison of the spike sequence of the PS (blue) and P14 (black) HAstV-VA1 strains. Amino acid differences are highlighted in cyan in the PS sequence. A composite of all escape mutations described in this work (mP14) is shown in green lettering. The escape mutations are highlighted in green.

presence of IgG antibodies to the recombinant P14 VA1-gastro spike in 180 serum samples collected from healthy persons (mean age 41 years; range 5–85 years) who participated in different population-based serosurveys conducted in Mexico (22) was evaluated by an ELISA (Fig. 8A). Since no *bona fide* HAstV-VA1-negative human sera were available, the OD values of each serum obtained against bovine serum albumin (BSA) in the ELISA were used as a negative control for each individual serum. As shown in Fig. 8A, the values obtained against the VA1 spike were significantly higher than those obtained to BSA (Mann-Whitney U test, *P*-value <0.05). Sera with OD values >0.3174 (upper limit of 95% CI: 0.2660, 0.3174) were considered positive for anti-VA1 antibodies, according to a conservative outlier threshold (Q3 + 2 × IQR) estimated for the control statistical distribution with 10,000 bootstrap iterations (Fig. 8A). The ELISA data revealed that 90.86% (upper limit of 95% CI: 94.62, 90.86%) of the samples showed OD values above

A

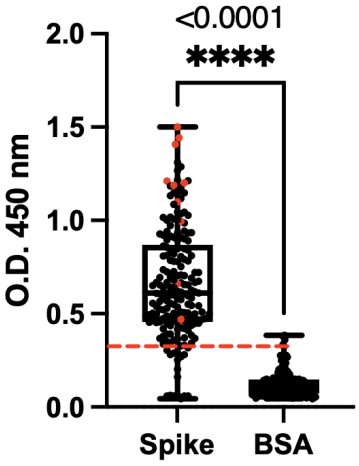

B

Human serum	ELISA O.D. 450 nm	Nt-titer wt VA1	Nt-titer TEM VA1	Fold difference Nt titer wt/TEM VA1
20	1.501	1:3,200	1:800	4
25	1.408	1:51,200	1:25,600	2
27	1.442	1:6,400	1:3,200	2
30	1.099	1:25,600	1:12,800	2
35	0.661	<1:200	<1:200	0
50	1.211	1:6,400	1:1,600	4
55	1.201	1:1,600	1:1,600	0
60	0.996	1:6,400	1:3,200	2
72	1.19	1:12,800	1:1,600	8
74	0.469	1:200	<1:200	>=2
Anti-VA1 (rabbit)	ND	1:6,400	1:1,600	4
Anti-spike (mouse)	ND	1:12,800	1:3,200	4

C

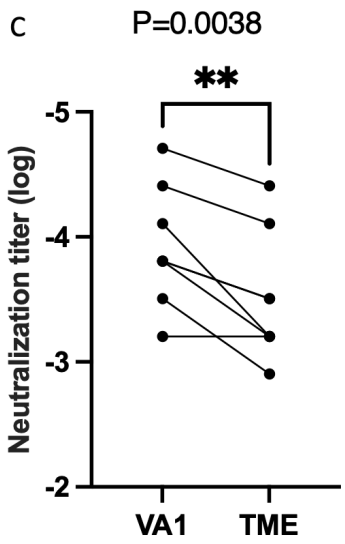

FIG 8 Titers of total and neutralizing human antibodies to HAstV-VA1. (A) The P14 recombinant spike was immobilized on ELISA plates and then incubated with a 1:100 dilution of a set of 180 human sera. Bovine serum albumin was used as a negative control for each serum instead of the VA1 spike. The antibody-antigen interaction was determined as described in Materials and Methods, and the optical density of the developed color was determined at 450 nm (OD 450). Each dot represents an individual serum, and the red dots represent the sera further analyzed by neutralization. The experiment was performed as two biological duplicates carried out in duplicate. The data are shown as a box and whisker plot. Significance was determined by the Mann-Whitney U test (****, $P < 0.0001$). The dotted red line represents the cut-off value of 0.3174, according to a conservative outlier threshold (Q3 + 2 × IQR) estimated for the control statistical distribution with 10,000 bootstrap iterations. (B) Wild-type and triple-escape mutant (TEM) HAstV-VA1 were incubated with a 1:100 dilution of selected human sera or rabbit and mouse polyclonal serum, and the virus's infectivity was determined as described in Materials and Methods. The neutralization titers are the serum dilution that neutralizes 50% of the VA1 infectious foci. The infectivity assay was performed in biological triplicates and carried out in duplicate. (C) Graphical representation of the data shown in (B). The neutralization titer values of each serum against the wild-type and triple-escape mutant are connected by lines. Significance was determined by a Wilcoxon matched-pairs signed rank test (****, $P < 0.0001$).

the median, consistent with a previous human serological study that showed a high seroprevalence for HAstV-VA1 (8). From this set of samples, we selected eight with the highest OD values and two with the lowest OD values (Fig. 8A) to determine their neutralization titer against the wild-type VA1-P14 strain and the triple-escape mutant VA1-P14 by a focus reduction assay. We found that the neutralization titers of this group of sera ranged from <1:200 to 1:51,200 (Fig. 8B). The neutralization titers observed for wild-type VA1 with the different sera were reduced on average 2.6-fold when tested against the triple-escape mutant VA1, and this difference was statistically significant (Fig. 8C). These results suggest that the neutralization sites identified in the HAstV-VA1 spike with the mice MAbs isolated in this study are also the target for the human-neutralizing immune response during natural infections with this virus.

DISCUSSION

We have previously identified five neutralization epitopes on the virus spike of classical HAstVs through mapping antibody escape mutations (17). All these mutations were subsequently shown to lie in the epitope footprint of the cognate Nt-MAb by X-ray crystallography and cryoelectron microscopy analyses of the antibody-spike complexes [(18); unpublished data], suggesting that escape mutations can indeed be a proxy reference site for the Nt-MAb-binding epitopes on the astrovirus spike domain. In this work, we have isolated and mapped mutations that allow HAstV-VA1 to escape neutralization by Nt-MAbs. As with the classical HAstVs, the escape mutations are located on the capsid spike domain of HAstV-VA1. In agreement with this observation, polyclonal antibodies raised against the recombinant spike domain, but not those elicited by the

core domain, induced high titers of Nt-Abs (Fig. 1B), as previously reported for classical HAstVs (17).

The HAstV-VA1 Nt-MAb escape mutations identified three independent neutralization epitopes that appear to be located in two different antigenic sites or regions that contain overlapping epitopes recognized by different antibodies. One antigenic site would be represented by the binding site of MAb 7C8 and the second by MAbs 2A2 and 3D8. These two sites are present on the same face of the spike but on opposite spike protomers. However, it cannot be discarded that some escape mutations may indirectly impact MAb neutralization by causing allosteric alterations that prevent the MAbs from binding to the virus, as has been shown for the gp120 spike protein of human immunodeficiency virus 1 (23) and the norovirus P domain (24). Of interest, the potential epitopes defined by the escape mutations are highly conserved among the sequences of both VA1-gastro and VA1-neuro strains deposited in public databases [see Fig. 5 in reference (9)], suggesting a function of these sites during virus infection.

Classical and VA viruses represent two different HAstV clades. However, although their spike proteins have low-sequence identity and apparent structural differences (9), they share a folding topology and a dimeric structure, which are also maintained in the MLB1 spike (25) and the recently described spike structure of murine astrovirus (26). In this regard, the previously reported escape mutations to Nt-Abs directed to classical HAstV serotypes 1, 2, and 8 (17) seem to lie in regions similar to those described in this work for the HAstV-VA1 spike (Fig. 9A and B). Thus, the neutralization epitope potentially recognized by the HAstV-VA1 Nt-MAb 7C8 seems to lie, topologically, very close to the epitope recognized by Nt-MAb 2D9 on the HAstV-8 spike, probably defining a similar antigenic site. Also, the epitopes recognized by MAbs PL2 and 3E8 on HAstV-2 and HAstV-8, respectively, represent, topologically, a similar antigenic site to that defined by HAstV-VA1 MAbs 2A2 and 3D8. In addition, MAbs 3B4 and 4B6, to HAstV-1 and HAstV-2, appear to form an additional antigenic site at the top of the spike. Finally, and very

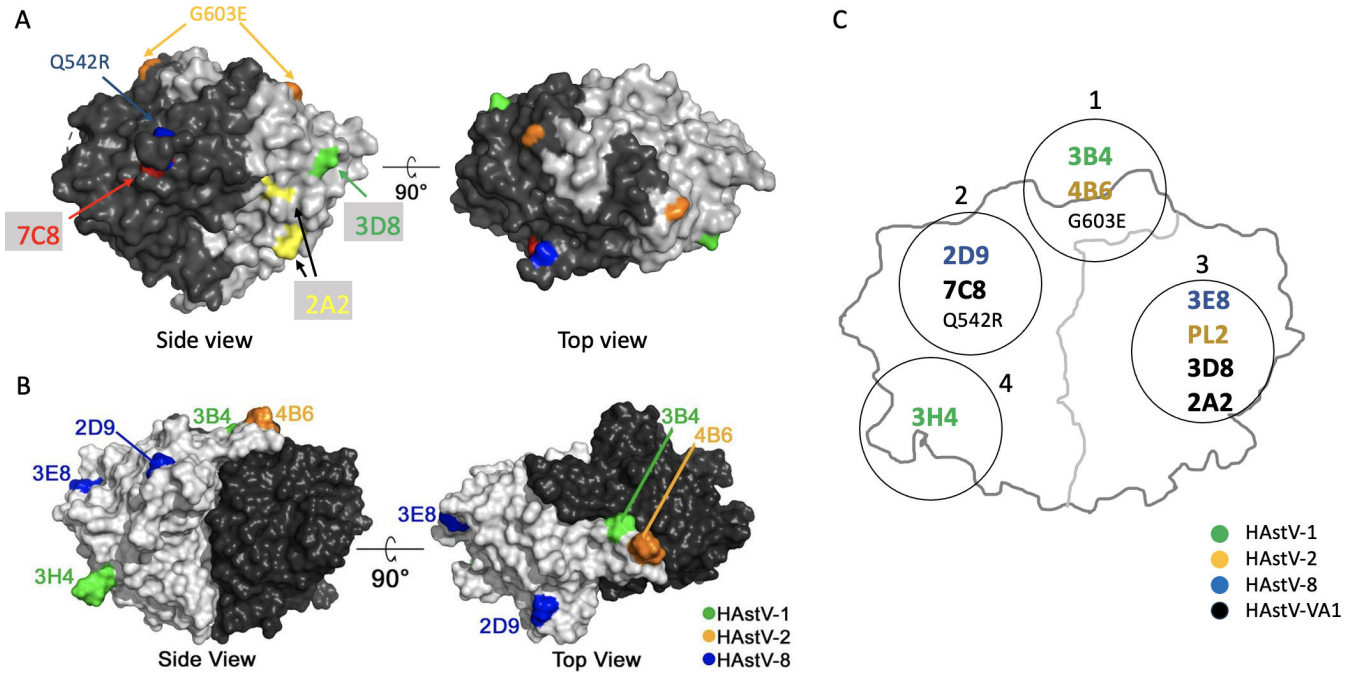

FIG 9 (A) Crystal structure of the HAstV-VA1 spike domain. The mutations that allow wild-type HAstV-VA1 to escape neutralization from the various MAbs are shown in different colors. The additional mutations identified in the double m7C8/2A2 and triple m7C8/2A2/3D8 escape mutants are in blue and orange, respectively. (B) The mutations that allow HAstV-1, -2, and -8 to escape neutralization [see reference (17)] are indicated in the crystal structure of the HAstV-2 spike domain. Both crystal structures are shown from the top and the side. Half of the dimers are colored dark gray and the other half light gray. In both structures, the mutations are shown in only one protomer in the dimer. (C) Diagrammatic scheme of the HAstV-2 spike domain. The circles represent the proposed antigenic domains, with the various Nt-MAb escape mutations indicated inside the circles.

interestingly, the epitope recognized by MAb 3H4 to HAstV-1 seems to represent an entirely different neutralizing antigenic site located in the lower region of the spike (Fig. 9B). Altogether, the neutralization escape mutations in both classical and HAstV-VA1 virus suggest the existence of at least four neutralization antigenic sites on the astrovirus spike domain, located in either of the two protomers and at the lower, middle, or top regions of the dimeric structure (Fig. 9C), highlighting the vulnerability of astrovirus to neutralization by the antibody immune response.

Two sites conserved on the spike of the eight classical HAstVs have been proposed as potential binding sites for a cell receptor (27). One of them, the P site located on the side of the spike, is in a similar location to that of the conserved C site identified when 15 different mouse astrovirus spike sequences were compared (26). These topologically conserved sites in classical human and murine astroviruses seem to overlap with the antigenic site 2 proposed in this work (Fig. 9C). On the other hand, the conserved S site in classical HAstVs (27) appears to overlap with antigenic site 4 (Fig. 9C). These regions may represent functional sites conserved among different astrovirus species and could underline the risk of transmission of animal AstVs to humans. It will be interesting to determine if the MAbs reported in this work neutralize the infectivity of the virus in cell lines different from Caco-2 cells; this information would be valuable to explore the generic function of the identified sites and potential alternate VA1 entry pathways.

In 2010, the spike sequence of a HAstV-VA1 strain (Genbank accession #ADH93577.1), obtained from a frontal cortex biopsy specimen (21), was reported. This specimen was detected in a 15-year-old boy with agammaglobulinemia who developed fatal astrovirus encephalitis. Notably, the patient received monthly intravenous immunoglobulin therapy during hospitalization. The amino acid sequence of the spike domain of this virus, HAstV-VA1-PS, has 21 amino acid changes compared to the sequence of the HAstV-VA1-P14 virus in our lab (Fig. 7B). Remarkably, two of these changes, Q542R and P543L, which are otherwise conserved in all HAstV-VA1 capsid sequences reported thus far (9), are identical to escape mutations selected by Nt-MAb in this work. In addition, a second amino acid change in the VA1-PS spike, T613V, lies between amino acids 611 and 615, the two changes selected in the escape mutant to Nt-MAb 2A2 (Fig. 7B). Altogether, these observations strongly suggest that the highly mutated VA1-PS strain, compared to the VA1-P14 strain, and in particular some of the mutations in the spike domain sequence, might have arisen due to the immune pressure imposed by the immunoglobulin therapy given to the patient. Immune pressure has also been suggested as an explanation for the emergence of the first SARS-CoV-2 variant of concern, Alpha (28, 29), and for the appearance of the original Omicron variant and its descendent BA.2.86, hypermutated variants, which most likely appeared in patients who received immunotherapy with convalescent plasma (30–32).

We also showed here that the neutralization antigenic sites reported in this work could be the target of neutralizing antibodies in humans during natural infections with the VA1 virus, supporting a relevant functional role of these sites in the HAstV spike during infection of the susceptible epithelial gastrointestinal cells. Moreover, the finding that the neutralization antibody titers to wild-type HAstV-VA1 in a set of human sera (Fig. 8B and C) had a 2.6-fold reduction when tested against the triple-escape mutant of the VA1 virus suggests that the antigenic sites represented by MAbs 7C8, 2A2, and 3D8 are immunodominant during a natural human VA1 infection. It remains to be determined if these sites on the virus overlap with binding sites for the cell receptor or co-receptors. In this regard, it has recently been reported that the neonatal Fc receptor (FcRn) facilitates classical HAstV cell infection at a post-binding step (33). However, FcRn does not seem involved in HAstV-VA1 infection [(33); unpublished data]. Determining the structure of the FcRn-HAstV spike complex and the effect of Nt-MAbs on the spike-FcRn interaction will help understand the neutralization mechanism of the reported antibodies to classical HAstVs. It should also give insights into the functional regions of nonclassical VA and MLB viruses.

The characterization of the neutralization mechanisms of the reported anti-VA1 Nt-MAbs, together with the identification of the actual epitopes of the antibodies on the virus spike by structural biology approaches, as has been previously shown for classical HAstV-8 (18), will aid in identifying virus functional sites required for astrovirus cell entry. This information will be relevant for developing prophylactic and therapeutic approaches to address this neurotropic astrovirus strain.

MATERIALS AND METHODS

Cells and viruses

Caco-2 cells, clone C2Bbe1 (ATCC), were propagated in DMEM Advanced (Gibco No. 12491015) supplemented with 5% fetal bovine serum (Cansera) and glutamine 2 mM in a 10% CO_2 atmosphere at 37°C. HAstV-VA1 was obtained from David Wang (Washington University, St. Louis, Missouri). The origin of classical HAstV serotypes 1, 2, and 8 has been reported (17). HAstV MLB1 was obtained from Susana Guix (Department de Microbiologia, Facultat de Biologia, Universitat de Barcelona). HAstV-VA1 was purified by isopycnic gradient centrifugation as previously described (15).

Recombinant proteins

Expression and purification of PS and P14 HAstV-VA1 spikes were carried out as previously described (9). Proteins containing amino acids 71–406 (DB), 180–300 (core), and 408–684 (spike) of VA1 ORF2 (GenBank #NC_013060.1) were synthesized in *E. coli* and purified as previously reported (15). The recombinant DB protein folds into the core structural domain that forms the capsid icosahedral shell.

Antibodies

Recombinant proteins representing different regions of the VA1 capsid precursor protein (described above; the spike protein sequence corresponds to the P14 strain) were used to generate hyperimmune sera in New Zealand rabbits, as reported previously (17). Rabbit and BALB/c mouse hyperimmune sera to VA1 were generated by immunization with either 250 ug (rabbits) or 50 ug (mice) of purified virus particles in Freund's complete adjuvant followed by three immunizations every 2 weeks, with the same amount of virus in Freund's incomplete adjuvant. Nt-MAbs 3B4, 4B6, and 2D9 to classical HAstV serotypes 1, 2, and 8, respectively, have been described (17).

Monoclonal antibody isolation and typing

Eight-week-old BALB/c mice were immunized with 50 ug of purified VA1 virus at 1:1 with Freund's complete adjuvant, and three more immunizations were performed every 2 weeks using the same amount of virus in Freund's incomplete adjuvant. Four days after the last immunization, the spleen was extracted, and splenocytes were fused with Fox myeloma cells using 50% polyethylene glycol; the cells were suspended in hypoxanthine-aminopterin-thymidine medium and directly plated in 96-well plates. Hybridomas-secreting antibodies to HAstV-VA1 were screened by an ELISA (see below), and those positive by the ELISA were then tested in a neutralization assay (see below). The hybridomas of interest were cloned three times by limiting dilution using peritoneal macrophage feeder layers. Selected MAbs were amplified as mouse ascitic fluid. The MAbs isotypes were determined using the RapidGet ELISA Mouse Antibody Isotyping Kit (Creative Diagnostics, New York) following the manufacturer's directions.

ELISA

Hybridomas positive for monoclonal antibodies to VA1 were selected using purified VA1 virus particles at a 2 ug/mL concentration in 96-well ELISA microtiter plates. Briefly, after virus adsorption, the plates were washed with PBS containing 0.1% Tween 20 and blocked with 1% BSA in PBS/Tween for 1 h at 37°C. Conditioned medium from

hybridoma cells or mouse hyperimmune serum was added as a control and incubated at 37°C for 1 h. After washing the plates, they were incubated with goat anti-mouse antibody conjugated to alkaline phosphatase (KPL). The reaction was developed by adding the phosphatase substrate (Sigma 104; 1 mg/mL), and the absorbance was recorded at 450 nm. In the case of human sera, the above procedure was followed, except that the VA1 P14 spike, or BSA as negative control, was used as antigen, and the sera were tested at a 1:100 dilution. A secondary anti-human IgG coupled to peroxidase (Aviva SB) was added at a dilution of 1:1,000 in PBS.

Immunofluorescence

Caco-2 cells grown on coverslips were infected with HAstV-VA1 at a multiplicity of infection (MOI) of 0.5. At 24 hpi, the cells were fixed with 2% paraformaldehyde in PBS for 20 min and permeabilized by incubation with 0.5% Triton X-100 in blocking buffer (1% BSA in PBS with 50 mM NH_4Cl) for 15 min. After washing with PBS, the coverslips were incubated with 3H4 (1:2,000), 2A2 (1:2,500), 7C8 (1:2,000), or 3D8 (1:1,000) MAb ascitic fluids for 1 h at room temperature. The cells were then washed with PBS, and Alexa 488-labeled anti-IgG antibody (Invitrogen) was added at a 1:1,000 dilution for 1 h at room temperature. Nuclei were stained with 30 nM DAPI (4=,6-diamidino-2-phenylindole) for 15 min. Coverslips were mounted on glass slides with Citifluor AF100 antifade solution (Citifluor Ltd., London, United Kingdom), and the samples were observed under a Zeiss Axioskop 2 fluorescence microscope coupled to a digital camera (Photometrics Cool Snap HQ).

Neutralization assays

The indicated concentration of ascitic fluid, hyperimmune sera, or human sera was preincubated at an MOI of 0.004 of wild-type, single-, double-, or triple-escape mutants of HAstV-VA1 strain for 1 h at room temperature. The virus-antibody mixture was then added to confluent C2Bbe1 cell monolayers grown in 96-well plates and incubated for 1 h at 37°C. After this time, the cells were washed three times with minimum essential medium without serum, and the infection was left to proceed in DMEM-HG supplemented with non-essential amino acids for 24 h at 37°C. Infected cells were detected by an immunoperoxidase focus-forming assay, as described previously (15) but using the anti-VA1 polyclonal antibody diluted 1:2,000 for detecting the viral antigens. The neutralization antibody titer was defined as the antibody dilution that blocks at least 50% of the input virus.

Biolayer interferometry experiments

Biolayer interferometry data were collected on an Octet RED384 using the Data Acquisition Software (version 11.1.1.19), with the temperature set to 25°C and shaking at 1,000 rpm. BLI experiments were performed in assay buffer (PBS, 1% BSA, 0.05% Tween 20). Anti-Mouse IgG Fc Capture biosensors were hydrated in assay buffer for at least 10 min before starting the experiment. BLI experiments were performed as follows: (i) pre-hydrated AMC biosensors were dipped in assay buffer for 60 s to establish a baseline; (ii) biosensors were dipped into a 1:200 dilution of mAb 7C8, 2A2, or 3D8 ascites fluid in assay buffer for 120 s to load the mAb onto the biosensor; (iii) biosensors were dipped into assay buffer for 60 s to confirm stable mAb loading and establish a new baseline; (iv) mAb-loaded biosensors were dipped in wells containing 1:2 serially diluted HAstV-VA1 spike in assay buffer at the indicated concentrations for at least 300 s to determine the association rate; (v) biosensors are dipped in assay buffer for 600 s to determine the dissociation rate. Each curve was reference subtracted with a 0-nM HAstV-VA1 spike control and aligned to the baseline and dissociation steps for inter-step correction. A global association 1:2 bivalent analyte model using the Octet Data Analysis HT software v7 (Sartorius) accounted for the dimeric HAstV-VA1 spike. At least three curves were used to determine the on- and off-rate and calculate the dissociation constant (KD). Average KD values are reported as the mean of two independent experiments.

Sequencing

The nucleotide sequences of the wild-type or mutant VA1 spike were determined as reported elsewhere (17), using the following primers: 5-GTCCAATATCTAGTTTATG -3 (SpikeVA1up), corresponding to nucleotides 5259–5277 of HAstV-VA1 (accession number NC_013060), and 5-GGCGCAATTTTTTCTTGAC-3 (SpikeVA1lw), corresponding to nucleotides 6453–6471 of the virus genome. After PCR amplification, the product was sequenced using Sanger chemistry at the sequencing facility of the Instituto de Biotecnología, Universidad Nacional Autónoma de México.

Isolation of neutralization-escape variants

To select escape variants, viral lysates (with at least 10^7 focus-forming units /mL) were incubated with the appropriate MAb at a dilution of 1:100–1:1,000 of the ascitic fluid for 1 h at room temperature. The mix was then used to infect CaCo-2 cell monolayers grown in 6-well plates for 1 h at 37°C, and the unbound virus was removed by washing three times. The cell monolayers were incubated at 37°C for 72–96 h in DMEM-HG supplemented with non-essential amino acids and tetracycline (1 µg/mL), and the corresponding MAb diluted 1:1,000. Viral lysates were then prepared by three freeze-thawing cycles, and the procedure was repeated at least three times before confirming the phenotype. The phenotype of the variant viruses was evaluated by a neutralization assay, and the selection was repeated until the detection of the neutralization-escape variants (which usually took four or five passages in the presence of the Nt-MAb). The double- and triple-escape variants were selected as described above, starting with the single or double mutant instead of the wild-type virus.

Statistics

Statistical analysis was performed using GraphPad Prism 9.0.1 Software (GraphPad Software, Inc.).

ACKNOWLEDGMENTS

This research was partially supported by grants NIH R01 AI144090 to R.M.D. and C.F.A., CONACyT 302965 to S.L., and DGAPA IN210120 to T.L.

We are grateful to David Wang (Washington University) for kindly providing human astrovirus VA1 and Susana Guix (Universitat de Barcelona) for the gift of MLB1 HAstV. We thank Marco Espinoza for his help in cell culture, Rodrigo-García-López for his assistance in the statistical analyses, and Elizabeth Mata, Graciela Cabeza, and the animal house personnel for help during animal handling and immunization. We also thank Santiago Becerra Ramirez, Eugenio Lopez Bustos, and Jorge Arturo Yañez Ponce de León for their assistance in the sequencing core facility of the Instituto de Biotecnología.

AUTHOR AFFILIATIONS

[1]Departamento de Genética del Desarrollo y Fisiología Molecular, Instituto de Biotecnología, Universidad Nacional Autónoma de México, Cuernavaca, Morelos, Mexico
[2]Departamento de Medicina Molecular y Bioprocesos, Instituto de Biotecnología, Universidad Nacional Autónoma de México, Cuernavaca, Morelos, Mexico
[3]Department of Biomolecular Engineering, University of California Santa Cruz, Santa Cruz, California, USA
[4]Centro de Investigación sobre Enfermedades Infecciosas, Instituto Nacional de Salud Pública, Cuernavaca, Morelos, Mexico

AUTHOR ORCIDs

Susana López http://orcid.org/0000-0001-6336-9209
Rebecca M. DuBois http://orcid.org/0000-0003-4185-5673

Carlos F. Arias http://orcid.org/0000-0003-3130-4501

FUNDING

Funder	Grant(s)	Author(s)
HHS | NIH | OSC | Common Fund (NIH Common Fund)	R01 AI144090	Rebecca M. DuBois Carlos F. Arias
Consejo Nacional de Ciencia y Tecnología (CONACYT)	302965	Susana López
UNAM | Dirección General de Asuntos del Personal Académico, Universidad Nacional Autónoma de México (DGAPA)	IN210120	Tomás López

AUTHOR CONTRIBUTIONS

Inci Ramírez-Bello, Data curation, Formal analysis, Investigation, Methodology, Writing – review and editing | Tomás López, Data curation, Investigation, Methodology, Writing – review and editing | Rafaela Espinosa, Investigation, Methodology, Writing – review and editing | Anisa Ghosh, Formal analysis, Methodology, Writing – review and editing | Kassidy Green, Methodology, Writing – review and editing | Lidia Riaño-Umbarila, Investigation, Methodology, Writing – review and editing | Carlos Gaspar-Castillo, Resources, Writing – review and editing | Catalina Aguilera-Flores, Investigation, Methodology, Resources | Celia M. Alpuche-Aranda, Resources, Writing – review and editing | Susana López, Formal analysis, Investigation, Writing – review and editing | Rebecca M. DuBois, Conceptualization, Funding acquisition, Validation, Writing – review and editing | Carlos F. Arias, Conceptualization, Formal analysis, Funding acquisition, Investigation, Supervision, Writing – original draft, Writing – review and editing

DATA AVAILABILITY

All data are included in the paper, and the discussed data are available in GenBank.

ETHICS APPROVAL

The samples were collected in three population-based serosurveys conducted in Tapachula, Chiapas (Sep 2018), Puente de Ixtla, Morelos (Jun 2016), and Campeche y Hopelchén, Campeche (Jun 2017) (22). The participants were selected randomly, were older than 2 years, and had no fever or other clinical manifestation at the time of sampling. The patient blood sampling protocol was approved by the Research Committee of the Instituto Nacional de Salud Pública (protocol/approval number: 1498/CI-776-2017 and 1449/CI-279-2017). The authors state that all procedures contributing to this work comply with the ethical standards of the Helsinki Declaration of 1975, as revised in 2008.

REFERENCES

1. Black RE, Perin J, Yeung D, Rajeev T, Miller J, Elwood SE, Platts-Mills JA. 2024. Estimated global and regional causes of deaths from diarrhoea in children younger than 5 years during 2000-21: a systematic review and Bayesian multinomial analysis. Lancet Glob Health 12:e919–e928. https://doi.org/10.1016/S2214-109X(24)00078-0
2. Bosch A, Pintó RM, Guix S. 2014. Human astroviruses. Clin Microbiol Rev 27:1048–1074. https://doi.org/10.1128/CMR.00013-14
3. Cortez V, Schultz-Cherry SL. 2023. Astroviruses, p 59–74. In Howley PM, Knipe DM (ed), Fields virology, 7th ed, Vol. 3. Wolters Kluger.
4. Finkbeiner SR, Kirkwood CD, Wang D. 2008. Complete genome sequence of a highly divergent astrovirus isolated from a child with acute diarrhea. Virol J 5:117. https://doi.org/10.1186/1743-422X-5-117
5. Finkbeiner SR, Li Y, Ruone S, Conrardy C, Gregoricus N, Toney D, Virgin HW, Anderson LJ, Vinjé J, Wang D, Tong S. 2009. Identification of a novel astrovirus (astrovirus VA1) associated with an outbreak of acute gastroenteritis. J Virol 83:10836–10839. https://doi.org/10.1128/JVI.00998-09
6. Kapoor A, Li L, Victoria J, Oderinde B, Mason C, Pandey P, Zaidi SZ, Delwart E. 2009. Multiple novel astrovirus species in human stool. J Gen Virol 90:2965–2972. https://doi.org/10.1099/vir.0.014449-0
7. Holtz LR, Bauer IK, Jiang H, Belshe R, Freiden P, Schultz-Cherry SL, Wang D. 2014. Seroepidemiology of astrovirus MLB1. Clin Vaccine Immunol 21:908–911. https://doi.org/10.1128/CVI.00100-14
8. Janowski AB, Owen MC, Dudley H, López T, Espinosa R, Elvin-Lewis M, Colichon A, Arias CF, Burbelo PD, Wang D. 2021. High seropositivity rate

of neutralizing antibodies to astrovirus VA1 in human populations. mSphere 6:e0048421. https://doi.org/10.1128/mSphere.00484-21
9. Ghosh A, Delgado-Cunningham K, López T, Green K, Arias CF, DuBois RM. 2024. Structure and antigenicity of the divergent human astrovirus VA1 capsid spike. PLOS Pathog 20:e1012028. https://doi.org/10.1371/journal.ppat.1012028
10. Wildi N, Seuberlich T. 2021. Neurotropic astroviruses in animals. Viruses 13:1201. https://doi.org/10.3390/v13071201
11. Perez LJ, Forberg K, Cloherty GA, Berg MG. 2023. Temporal and coevolutionary analyses reveal the events driving the emergence and circulation of human mamastroviruses. Emerg Microbes Infect 12:2217942. https://doi.org/10.1080/22221751.2023.2217942
12. Donato C, Vijaykrishna D. 2017. The broad host range and genetic diversity of mammalian and avian astroviruses. Viruses 9:102. https://doi.org/10.3390/v9050102
13. Lukashov VV, Goudsmit J. 2002. Evolutionary relationships among *Astroviridae*. J Gen Virol 83:1397–1405. https://doi.org/10.1099/0022-1317-83-6-1397
14. Mendenhall IH, Smith GJD, Vijaykrishna D. 2015. Ecological drivers of virus evolution: astrovirus as a case study. J Virol 89:6978–6981. https://doi.org/10.1128/JVI.02971-14
15. Aguilera-Flores C, López T, Zamudio F, Sandoval-Jaime C, Pérez EI, López S, DuBois R, Arias CF. 2022. The capsid precursor protein of astrovirus VA1 is proteolytically processed intracellularly. J Virol 96:e0066522. https://doi.org/10.1128/jvi.00665-22
16. Bogdanoff WA, Perez EI, López T, Arias CF, DuBois RM. 2018. Structural basis for escape of human astrovirus from antibody neutralization: broad implications for rational vaccine design. J Virol 92:e01546-17. https://doi.org/10.1128/JVI.01546-17
17. Espinosa R, López T, Bogdanoff WA, Espinoza MA, López S, DuBois RM, Arias CF. 2019. Isolation of neutralizing monoclonal antibodies to human astrovirus and characterization of virus variants that escape neutralization. J Virol 93:e01465-18. https://doi.org/10.1128/JVI.01465-18
18. Ricemeyer L, Aguilar-Hernández N, López T, Espinosa R, Lanning S, Mukherjee S, Cuellar C, López S, Arias CF, DuBois RM. 2022. Structures of two human astrovirus capsid/neutralizing antibody complexes reveal distinct epitopes and inhibition of virus attachment to cells. J Virol 96:e0141521. https://doi.org/10.1128/JVI.01415-21
19. Bub T, Hargest V, Tan S, Smith M, Vazquez-Pagan A, Flerlage T, Brigleb P, Meliopoulos V, Lindenbach B, Ramanathan HN, Cortez V, Crawford JC, Schultz-Cherry S. 2023. Astrovirus replication is dependent on induction of double-membrane vesicles through a PI3K-dependent, LC3-independent pathway. J Virol 97:e0102523. https://doi.org/10.1128/jvi.01025-23
20. Guix S, Caballero S, Bosch A, Pintó RM. 2004. C-terminal nsP1a protein of human astrovirus colocalizes with the endoplasmic reticulum and viral RNA. J Virol 78:13627–13636. https://doi.org/10.1128/JVI.78.24.13627-13636.2004
21. Quan PL, Wagner TA, Briese T, Torgerson TR, Hornig M, Tashmukhamedova A, Firth C, Palacios G, Baisre-De-Leon A, Paddock CD, Hutchison SK, Egholm M, Zaki SR, Goldman JE, Ochs HD, Lipkin WI. 2010. Astrovirus encephalitis in boy with X-linked agammaglobulinemia. Emerg Infect Dis 16:918–925. https://doi.org/10.3201/eid1606.091536
22. Gaspar-Castillo C, Cortes-Escamilla A, Aparicio-Antonio R, Carnalla M, López S, Sánchez-Tacuba L, Oceguera-Cabrera A, Burrone Ó, González-Bonilla C, Ortiz Navarrete V, Martínez-Barnetche J, Rodríguez MH, Alpuche-Aranda CM. 2024. Evolution of Zika prevalence in a dengue hyper-endemic municipality in Southern Mexico after the outbreak of 2015 to 2017. Salud Publica Mex 66:218–225. https://doi.org/10.21149/15407
23. Sethi A, Tian J, Derdeyn CA, Korber B, Gnanakaran S. 2013. A mechanistic understanding of allosteric immune escape pathways in the HIV-1 envelope glycoprotein. PLoS Comput Biol 9:e1003046. https://doi.org/10.1371/journal.pcbi.1003046
24. Kolawole AO, Smith HQ, Svoboda SA, Lewis MS, Sherman MB, Lynch GC, Pettitt BM, Smith TJ, Wobus CE. 2017. Norovirus escape from broadly neutralizing antibodies Is limited to allostery-like mechanisms. mSphere 2:e00334-17. https://doi.org/10.1128/mSphere.00334-17
25. Delgado-Cunningham K, López T, Khatib F, Arias CF, DuBois RM. 2022. Structure of the divergent human astrovirus MLB capsid spike. Structure 30:1573–1581. https://doi.org/10.1016/j.str.2022.10.010
26. Lanning S, Pedicino N, Haley DJ, Hernandez S, Cortez V, DuBois RM. 2023. Structure and immunogenicity of the murine astrovirus capsid spike. J Gen Virol 104:001913. https://doi.org/10.1099/jgv.0.001913
27. Dong J, Dong L, Méndez E, Tao Y. 2011. Crystal structure of the human astrovirus capsid spike. Proc Natl Acad Sci U S A 108:12681–12686. https://doi.org/10.1073/pnas.1104834108
28. Corey L, Beyrer C, Cohen MS, Michael NL, Bedford T, Rolland M. 2021. SARS-CoV-2 variants in patients with immunosuppression. N Engl J Med 385:562–566. https://doi.org/10.1056/NEJMsb2104756
29. Rambaut A, Loman N, Pybus O, Barclay W, Barret J, Carabelli A, Connor T, Peacock T, Robertson DL, Volz E. 2020. Preliminary genomic characterisation of an emergent SARS-CoV-2 lineage in the UK defined by a novel set of spike mutations. Available from: https://virological.org/t/preliminary-genomic-characterisation-of-an-emergent-sars-cov-2-lineage-in-the-uk-defined-by-a-novel-set-of-spike-mutations/563. Retrieved 03 Feb 2024.
30. Berkhout B, Herrera-Carrillo E. 2022. SARS-CoV-2 evolution: on the sudden appearance of the Omicron variant. J Virol 96:e0009022. https://doi.org/10.1128/jvi.00090-22
31. CDC. 2023. Risk assessment summary for SARS CoV-2 sublineage BA.2.86 on centers for disease control and prevention. Available from: https://www.cdc.gov/respiratory-viruses/whats-new/covid-19-variant.html. Retrieved 03 Feb 2024.
32. Tan CW, Chia WN, Zhu F, Young BE, Chantasrisawad N, Hwa S-H, Yeoh AY-Y, Lim BL, Yap WC, Pada SKMS, Tan SY, Jantarabenjakul W, Toh LK, Chen S, Zhang J, Mah YY, Chen VC-W, Chen MI-C, Wacharapluesadee S, Sigal A, Putcharoen O, Lye DC, Wang L-F. 2022. SARS-CoV-2 Omicron variant emerged under immune selection. Nat Microbiol 7:1756–1761. https://doi.org/10.1038/s41564-022-01246-1
33. Haga K, Takai-Todaka R, Kato A, Nakanishi A, Katayama K. 2023. Neonatal Fc receptor is a functional receptor for human astrovirus. bioRxiv. https://doi.org/.org/10.1101/2022.11.13.516297